Fibers and Polymers 2019, Vol.20, No.11, 2390-2399
DOI 10.1007/s12221-019-1194-9

ISSN 1229-9197 (print version)
ISSN 1875-0052 (electronic version)

Failure Analysis of CFRP Multidirectional Laminates Using the Probabilistic Weibull Distribution Model under Static Loading

Alok Behera*, Manjusha M. Thawre, and Atul Ballal

Department of Metallurgical and Materials Engineering, Visvesvaraya National Institute of Technology (VNIT), Nagpur 440010, India

(Received December 13, 2018; Revised May 17, 2019; Accepted May 23, 2019)

Abstract: The application of carbon fiber reinforced polymer (CFRP) Multidirectional (MD) laminates in aircraft structure have motivated the manufacturers to tailor the mechanical strength in desired directions. The complex stress field owing to multiple orientations with the loading direction increases the intricacy of failure analysis. Hence, the macroscopic and microscopic fracture behaviour of MD CFRP laminates under static loading needs to be explored further. In this study, four different MD CFRP laminates were fabricated using IMA/M21 prepregs by the autoclaving technique. Effect of fiber orientation on static strength i.e. tensile and compressive strength was studied. The strength decreased with the increase in orientation angle. Scanning electron micrographs revealed that irrespective of the lay-up sequence individual layers failed parallel to the fiber direction. Fiber breakage and delamination were the major failure modes in tensile specimens while kinking, matrix failure, in-plane shear, stepped fracture, and fiber-matrix debonding were dominated in compression specimens. The theoretical and experimental data was in good agreement with the Weibull distribution model.

Keywords: CFRP, Multidirectional, Tensile strength, Compressive strength, SEM

Introduction

Carbon fiber reinforced polymer (CFRP) composite is a leading high-performance material that has outperformed the functionality, properties, cost and durability of traditional materials. In recent years application of CFRP has increased in sectors such as wind energy, sporting goods, automobiles, defence, aircraft, etc. It is widely used as aircraft structural components which undergo severe cyclic loading in multiple directions during their service life. Fiber reinforced polymer (FRP) composites accounted for approximately 53 wt. % of Airbus 350 XWB that resulted in improved performance, lower maintenance and up to 25 % fuel saving through weight reduction.

Geometrical parameters (thickness, number of layers, lay-up sequence) and loading parameters (type, magnitudes, frequency, loading axis) governs the mechanical behaviour of polymer composites [1-3]. Numerous researchers had correlated the dependence of strain rate, temperature, fiber volume, macroscopic deformation and orientation of composites [4-6]. Based on orientation, CFRP laminates can be unidirectional (UD), Off-axis or multidirectional (MD). This loading direction-based uncertainty makes UD inappropriate for structural applications and brings in development of rest two. Anisotropic UD showed lower transverse strength as compared to longitudinal strength due to its inner structure [7].

The off-axis laminates were fabricated either by cutting UD or else by placing lay-ups at desired orientations. The difference between tensile and compressive strength of Off-axis laminates increased with increase in off-axis angle [8-12]. The tensile strength reduced drastically up to 15^{o} off-axis angle and remained constant with further increase of angles [13-16]. The variation between off-axis compressive and tensile strength magnitude mostly rely on the fiber orientation and this phenomenon was named as off-axis strength differential (SD) effect [17]. The static strength variation was due to nonlinear deformation, shear deformation of the weak polymer matrix, existing defects during fabrication and irregularity in sample preparation, etc. Maintaining a favorable 2-D stress field with the off-axis orientation of fibers was very difficult and even slight inclination in fixturing or tabbing generates a complex state of stress which leads to premature failure.

Evolution of MD laminates has partially resolute the anisotropy of UD and off-axis laminates by keeping various layers at desired orientations [18]. Under realistic service conditions, MD structural components were prone to complex fatigue loading having variable parameters like amplitude, mean, frequency and waveform [19,20]. The failure mechanisms of UD and off-axis laminates were vital to analyze the strength and fracture of MD laminates. The fracture analysis usually involved the individual response of fiber, matrix and fiber-matrix interface once loaded. Multiple orientations generated a triaxial state of stress that made the failure more complex. The failure under Static loading often initiated as transverse matrix crack in off-axis plies [21,22]. However, these cracks had a minor impact on stiffness degradation rather accumulated as a source for more critical failure like delamination or fiber failure [23,24]. The lower maximum principal stress than critical stress for orientation greater than 20^{o} resulted in fiber dominated failure [25]. The fiber-matrix interfacial resistance of MD was higher than UD laminates. The MD interface fractures were primarily

*Corresponding author: alokab132@gmail.com

caused due to nonlinear strain, pseudoplastic behavior of the matrix and ply stiffness mismatch [26].

Several 2D and 3D micromechanical models had been proposed to simulate the complex fracture of CFRP MD laminates. Deng *et al*. had analytically validated a few existing micromechanical models for nonlinear mechanical behavior of angle-ply laminates under tension [27]. Montesano *et al.* proposed a model to efficiently predict ply crack considering both intra-ply and inter-ply ply cracking and their interactions. The model also encountered combined stress state and 3D nature of ply constraining effects [28]. Meanwhile, improvement in fiber extraction and laminate fabrication techniques over time had changed the overall properties of composites. Hence, a detailed experimental analysis of failure modes in MD laminates needs to be investigated.

The two-parameter Weibull probabilistic model is a potential tool for reliability and failure distribution analysis for a wide horizon of specimens [29,30]. However, researchers had also used statistical Weibull distribution model with less number of samples effectively for analysis [31,32]. Although accuracy will be higher with a larger sample size. The characteristic strength/scale parameter (σ_o) and shape parameter (m) was vital to analyze the accuracy of experimental strength (σ). Wang *et al.* had observed changes in σ_o with variation in strain rate and temperature for E-glass composites, whereas m remained independent [33]. This Weibull reliability analysis proved to be a vital tool for design engineers to decide safe stress levels.

The present investigation experimentally analyzes the macroscopic and microscopic fracture behavior of carbon fiber/epoxy IMA/M21 prepreg MD laminates under tensile and compressive loading. Tests were carried out on four MD laminates with different lay-up sequence. The tensile and compressive strengths were compared with previous results for UD and off-axis laminates. The final failures were characterized by macroscopic and SEM micrographs. The Weibull probabilistic model was employed to analyze variation in tensile and compressive results.

Experimental

Material

The carbon fiber/epoxy IMA/M21 prepregs of 300 mm wide roll and 0.18 mm nominal thickness was brought from M/s Hexcel. IMA carbon fiber is extensively used in aircraft industries due to its high modulus, strength, and uniformity. It is a PAN-based surface-treated fiber with a filament count of 12000 (12K). Likewise, Hexply M21 epoxy matrix is an excellent transmitter of fiber properties with excellent toughness and high performance. The detailed mechanical properties of IMA carbon fiber and M21 epoxy matrix are given in Table 1. The prepreg was cut into 300 mm×450 mm layers and laid up at desired orientations as shown in Figure 1(a). Similarly, four different MD laminates were manufactured by varying the stacking sequence and number of layers with a constant fiber volume of 59 %. The autoclave curing was performed at 180 °C with 2 °C/minute heating rate and two hours holding time. A gauge pressure of 7 bar and full vacuum of 1 bar was maintained during curing. Finally, the cured laminates were cooled at room temperature. The laminate details are given in Table 2 where MD90, MD45, MD30 were symmetric while MDQI was quasi-isotropic.

Table 2. Laminate details

Lay-up sequence	No. of layers	Thickness (mm)	Laminate code
$(0,90,0,90)_{2S}$	16	3.10	MD90
$(+45,-45,+45,-45)_{2S}$	16	3.10	MD45
$(0,30)_{2S}$	8	1.61	MD30
$(+45,-45,0,90)_{2S}$	16	3.52	MDQI

Specimen and Experimental Procedure

Static tensile and compression test specimens were prepared as per ASTM D3039 [34] and ASTM D3410 [35] respectively. A rotary diamond cutter was used for sample preparation followed by polishing of thickness side to avoid any pre-existing defect. The gauge length for tensile and compressive specimen was 50 mm and 10 mm respectively as shown in Figure 1(b). Glass fiber end tabs of 50 mm length were fixed by means of Araldite to avoid slippage of the specimen in grips.

The tests were carried out on a universal testing machine (Make: Instron, Model: 8802, Capacity: 250 KN) at a constant crosshead speed of 1 mm/min. At least fifteen replicate samples were tested to confirm the average strength or even more to counter the associated scattering. Instron 2630-100 series clip-on extensometer having 25 mm gauge

Table 1. Properties of IMA carbon fiber and M21 epoxy resin

IMA carbon fiber		M21 epoxy	
Tensile strength	6,067 MPa	Flexural yield strength	147 MPa
Tensile modulus	297 GPa	Flexural modulus	3.50 GPa
Density	1.79 g/cm^3	Density	1.28 g/cc
Filament count	12000	Flexural strain at yield	5 %
Filament diameter	5.1 microns	Curing temperature	180 °C

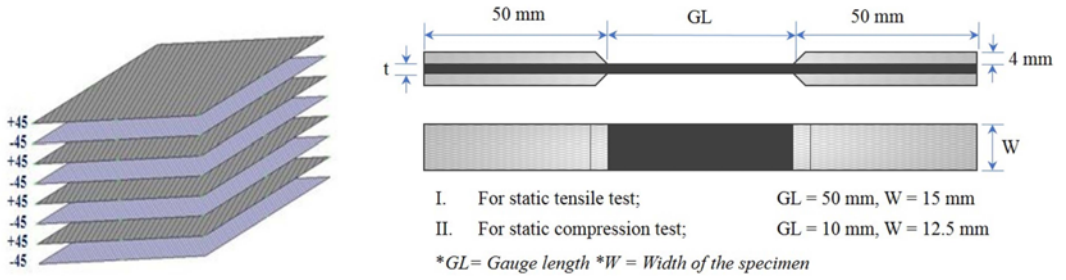

Figure 1. (a) Schematic of MD45 laminate and (b) specimen geometry for static testing.

length was used to measure the tensile strain. The microstructural characterization of the fracture surface was carried out using the JEOL 6380 scanning electron microscope (SEM). The samples were initially coated with a thin layer of platinum by auto sputter (Make: JEOL) to make it conducting. Subsequently, fracture behavior was examined using macroscopic and microscopic images.

Results and Discussion

Tensile Strength of MD Laminates

Longitudinal tensile properties of MD CFC laminates were fiber dominated and the stress-strain curve was linear till first notable damage, followed by a catastrophic failure. Nominal scatter was observed in ultimate tensile strength (UTS). The mean strength values, standard deviations, and coefficient of variation are given in Table 3. MD90 exhibited the highest strength due to fibers aligned along loading direction followed by MDQI, MD30, and MD45 respectively. The standard deviation and coefficient of variation (CV) as given in Table 3 showed the scattering in experimental tensile strength. The MD45 laminate showed the highest CV reflecting highly scattered data due to the presence of cross-ply layers. The strength of MD laminates drastically reduced with increase in off-axis angle and very similar trends were observed previously for off-axis laminates [14,16].

The stress-strain curves from the uniaxial tensile test are shown in Figure 2. The MD45 and MD30 slopes showed a bilinear stress-strain post 1 % strain. This large strain was suitable under monotonic loading condition while after 1 % strain a little load fluctuation leads to catastrophic failure. The 45 ^{o} or 30 ^{o} layer in a laminate undergoes varying ductile

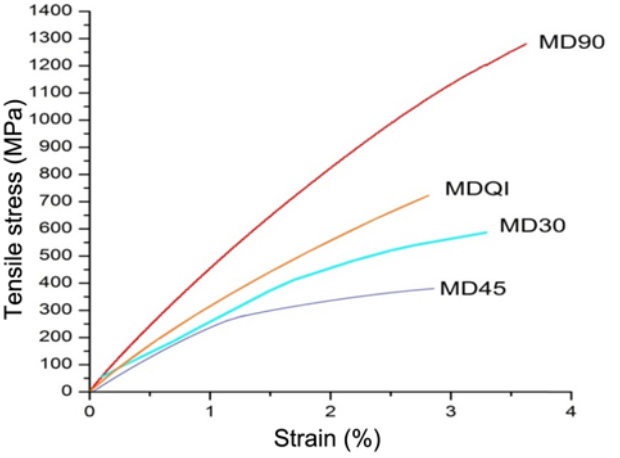

Figure 2. Stress-strain relationship of MD CFC laminates under tensile loading.

behavior post inflection point which was 1 % strain at present. In post inflection point phase, the off-axis layers with respect to loading direction tend to re-orient towards loading axis bringing fiber angle down. The growth of permanent strains before the inflection point was the reason behind the bilinear response. The stress increased rapidly during the initial 1 % strain followed by a brisk increase in strain up to 2.97 % for MD45 and 3.32 % for MD30 with an insignificant increase in stress. The re-orientation of fiber caused higher failure strain as compared to a 0 ^{o} UD laminate [36,37]. Hence, the reorientation of off-axis fibers during static loading was concluded to be the reason behind bilinear stress-strain response and high-straining ductile behavior [38]. However, the existence of 0 ^{o} and 90 ^{o} oriented layers in

Table 3. Tensile and compressive test result

Laminates	UTS (MPa)	Standard deviation (MPa)	Coefficient of variation (%)	Elongation (%)	UCS (MPa)	Standard deviation (MPa)	Coefficient of variation (%)	Elongation (%)
MD90	1292	28.12	2.17	3.66	612	10.89	1.78	0.026
MD45	250	13.24	5.29	2.97	165	6.48	3.92	0.074
MD30	584	3.79	0.65	3.32	214	7.03	3.28	0.097
MDQI	718	7.05	0.98	2.70	440	4.42	1.00	0.067

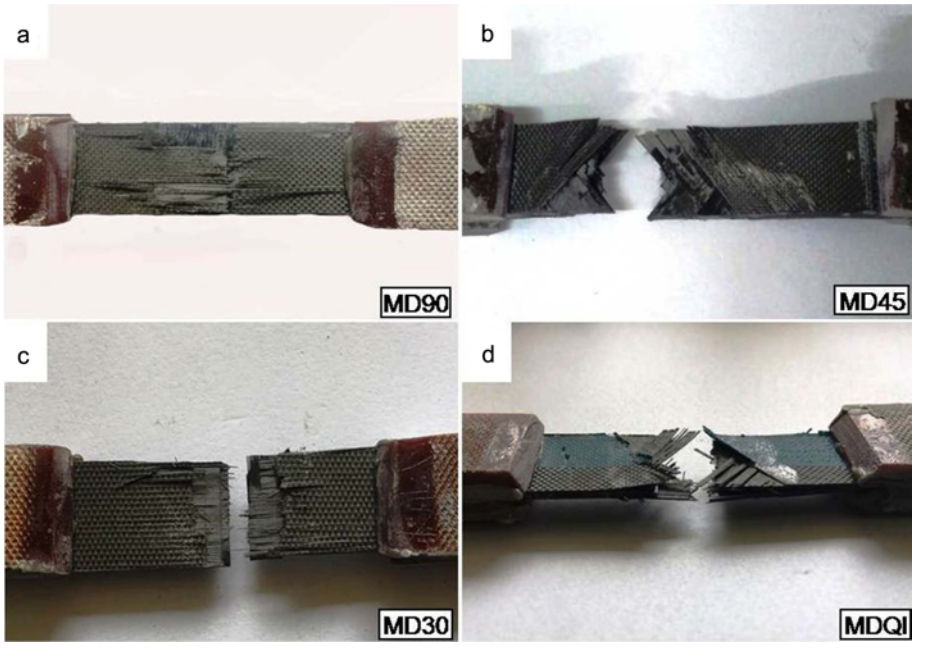

Figure 3. Tensile macroscopic failure mode observed in MD CFC laminates.

MD90 and MDQI laminates resulted in a noticeable linear stress-strain response as shown in Figure 2.

The tensile fracture morphology of MD laminates is shown in Figure 3(a-d). The fractured path was parallel to the fiber direction except for MD30 laminate. Regardless of orientation, layer-wise fracture morphology of MD was identical to off-axis laminates as reported earlier [13,39]. Initially, brittle matrix cracking was the dominating mode of fracture. However, the final fracture was always due to delamination and fiber failure. MD30 splitted close to tabs and parallel to the fiber direction without any clear delamination. This reflected an increase in shear stress and nonlinear stress-strain response. This phenomenon of combined split and fiber fracture was previously reported for orientation $\leq 30^{\circ}$ [25]. None of the tabs were separated or crushed during the tensile test which manifested the absence of tabbing stress in all the laminates.

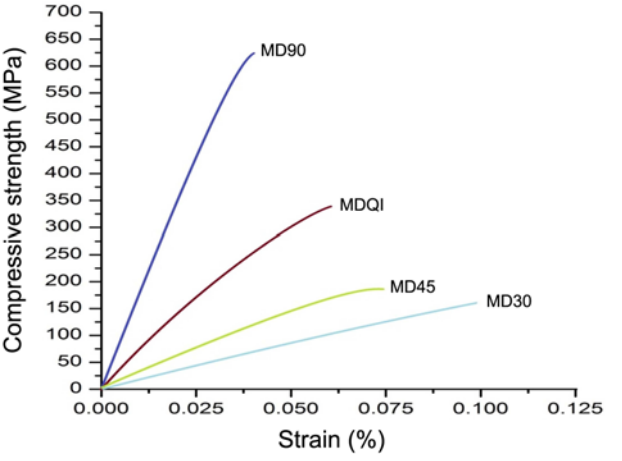

Figure 4. Stress-strain relationship of MD CFC laminates under compressive loading.

Compressive Strength of MD Laminates

The ultimate compressive strength (UCS) and % elongation at failure obtained are given in Table 3. The UCS was nearly half of the UTS value expect for MDQI laminate which reflects quasi-isotopic nature. The compression specimen followed trend of tensile tests where UCS was higher for laminates having fibers in loading direction i.e. MD90 and MDQI. As per literature, 30° off-axis laminates had higher compressive strength than 45°. Here, MD30 had higher compressive strength even if consists half layers then MD45 [40]. The MD45 and MD30 laminate showed the highest coefficient of variation reflecting scatted strength due to angled plies as given in Table 3. The compression stress-strain curves also followed a bi-linear relationship under compressive loading as shown in Figure 4. The change in loading pattern due to twisting or re-orientation of angle-ply fiber with increasing compression loading imposes the change in linearity. A linearity shift of compression stress-strain curve was also observed prior to final fracture for MD45 and MD90 laminates. This can be attributed to matrix dominated shear deformation just before the catastrophic fracture. The compression stress-strain diagram illustrated comparatively less fracture strain due to the ineffectiveness of fiber reorientation phenomenon as compared to tensile specimens. The effect of fiber orientation was insignificant

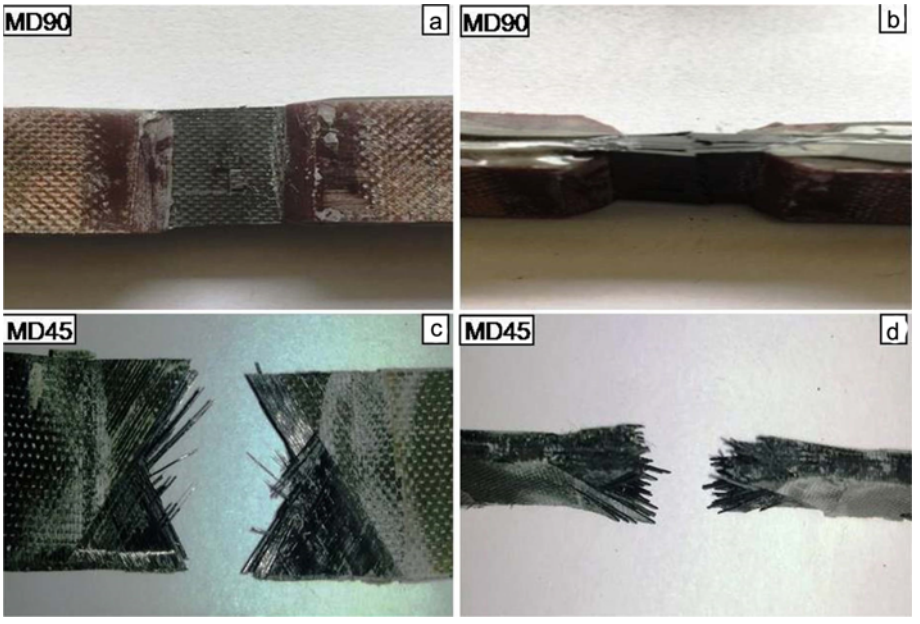

Figure 5. Compressive macroscopic failure mode observed in MD90 and MD45 laminates.

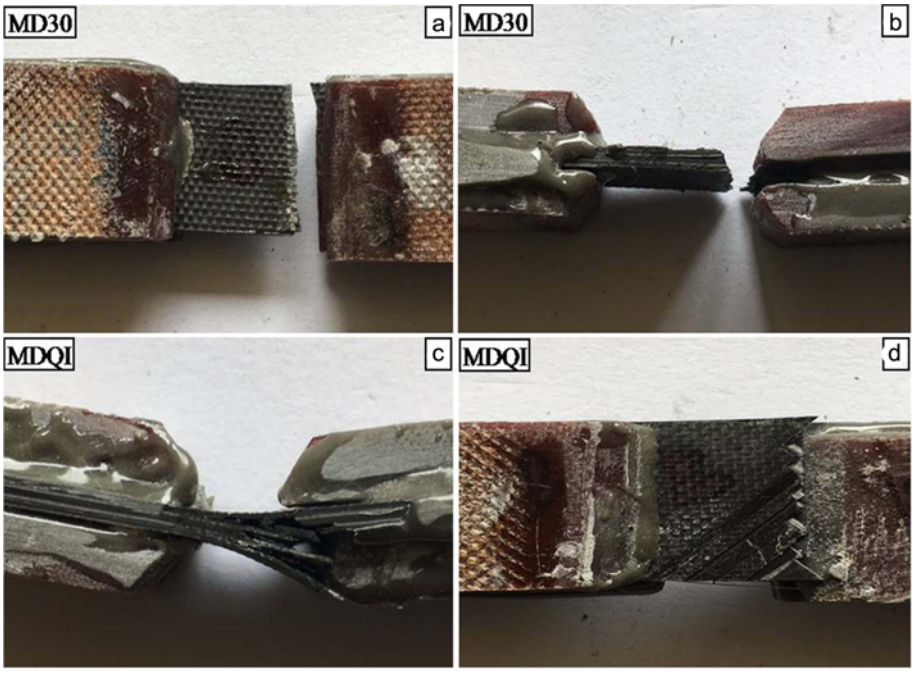

Figure 6. Compressive macroscopic failure mode observed in MD30 and MDQI laminates.

in compression loading due to matrix dominated brittle failure [38].

The compressive specimens fractured within the gauge length and tabs were separated in few specimens reflecting the existence of tabbing stress as shown in Figures 5, 6. This also confirmed the presence of high local stresses near the end tabs and premature failure [41]. The MD45 and MDQI end tabs were particularly removed as shown in Figure 5(c-d) and Figure 6(c-d) respectively. In MDQI laminate the $\pm 45^{\circ}$ layers provided lateral support to crack formation in 90° and 0° layers. The lateral support delays propagation of cracks in the orientated layer, which generates undesirable stress near the end tabs. The longitudinal cracks finally resulted in in-plane kink band. This delayed the initiation of

fiber micro-buckling, crack propagation and dynamic stress field. This delay results in higher compressive strain in MD as compared to UD laminates [41].

Macroscopic failure of tensile and compression specimens was identical in two aspects. Firstly, the fracture was parallel to fiber orientation and secondly, fracture surface was inclined to the through-thickness surface. The tensile fracture was dominated by fiber failure, delamination, and interface debonding, etc, whereas compressive failure was either due to in-plane or out-of-plane shear mode failure. Therefore, it was concluded that tensile failure predominantly depends on fiber properties whereas compressive failure relies heavily on the matrix and fiber-matrix interface.

SEM Morphology of Tensile Fracture Specimen

The scanning electron micrographs were obtained from fracture surface of tensile specimens. Thy criss-cross layup confirmed parallel to fiber direction failure for all the MD laminates as shown in Figure 7(a-d). The micrograph of MDQI showed an independent +45, -45, 0, 90 layers along with delamination and fiber failure as depicted in Figure 7(d). Figure 7(e) showed the resin rich area and matrix crack formation in the MD90 laminate, where a bunch of fiber had broken near the crack accumulation point. The fiber breakage and fiber-matrix debonding were found at higher magnification for MDQI laminates as shown in Figure 7(f). The Surface morphology of tensile specimens revealed that failure usually began with matrix cracking and fiber-matrix debonding, whereas the final failure was always due to fiber breakage, delamination or fiber pullout irrespective of the orientation. Single fiber failure followed a statistical distribution with final failure of the laminate. Failure of solo or bunch of fibers acted as local damage that led to improper stress distribution between fiber and matrix. Hence, this fiber breakage at the beginning of the test reduced the fracture resistance of laminate.

SEM Morphology of Compressive Fracture Specimen

MD compressive specimens failed with an audible noisy event followed by instantaneously catastrophic failure. The broken surface was inclined to width direction referring to in-plane micro-buckling or in-plane shear. This micro-buckling ultimately resulted in delamination through the interface, fiber-matrix debonding and wedge-shaped failure

Figure 7. SEM micrographs of tensile fractures.

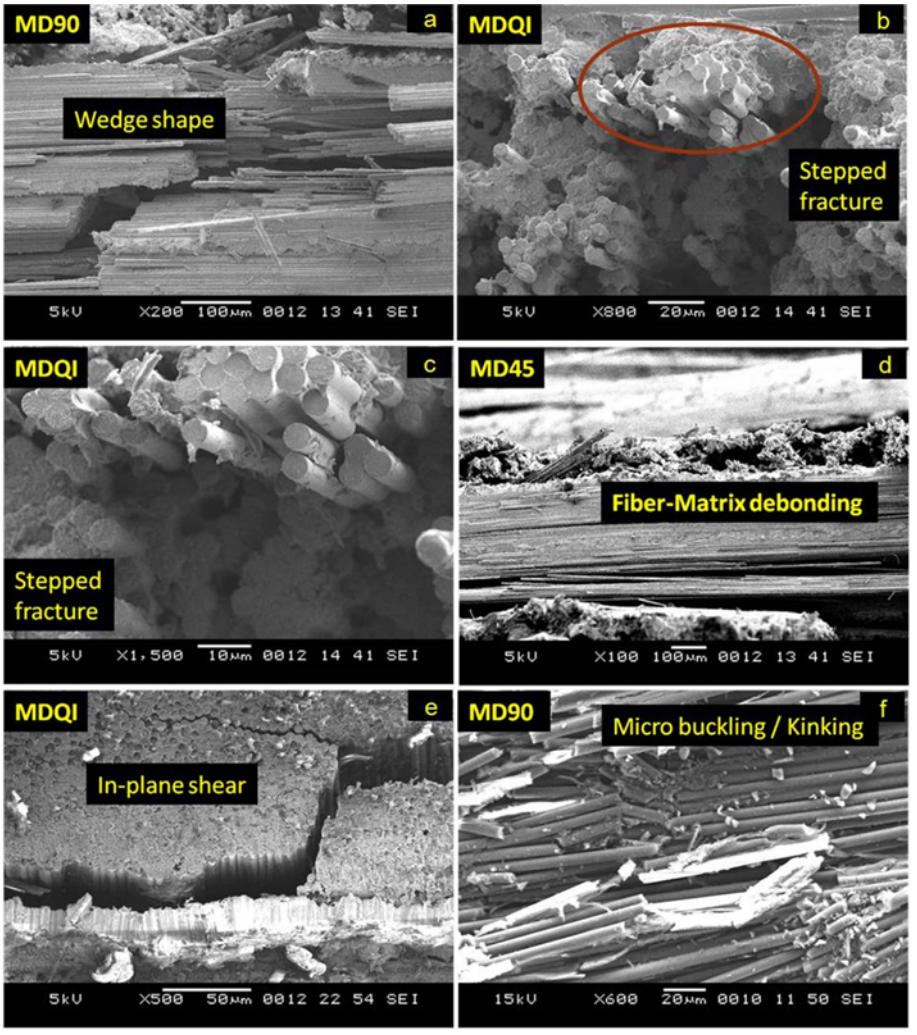

Figure 8. SEM micrographs of compressive fractures.

as shown in Figure 8(a, d and e). Similarly, Figure 6(b) showed the Inclined failure to the thickness direction called as out-of-plane micro-buckling [41]. A complete change in compressive fracture morphology with an increase in off-axis angle (θ) was reported previously. The initiation of fracture in compressive loading was dominated by interlaminar shearing, in-plane matrix shearing, and matrix compression for orientation range of ($0^{o} < \theta < 15^{o}$), ($15^{o} < \theta < 50^{o}$), ($50^{o} < \theta < 90^{o}$) respectively [24]. A similar trend of matrix dominated failure was observed here for all the MD laminates where orientations were higher than 15^{o}.

Formation of kink band was vital in a longitudinal compressive fracture where ductile fiber fails in a brittle manner as shown in Figure 8(f). Any misalignment or fiber waviness instantly triggered fiber buckling leading to kinking failure. The fiber waviness had been almost eliminated in modern curing techniques like Vacuum Enhanced Resin Infusion Technology (VERITy) which further reduced the probability of kinking. Combined micro-buckling and kinking caused stepped fracture as shown in Figure 8(b). The enlarged view of stepped fracture at 1500 magnification also showed fiber breakage and fiber-matrix debonding as shown in Figure 8(c).

Weibull Analysis

In the present study, the Weibull model was used to analyze variation in tensile and compressive results of four different MD laminates. The Weibull median rank estimator was used to evaluate the cumulative probability density (P_f) where i was current test number and n was the total number of tests performed as given in equation (1) [29,30]. For all MD laminates i=A number between 1 to 15 and n=15 were taken for calculations. The intercept (c), shape parameter (m) and the scale parameter (σ_o) were evaluated with the known value of (σ) and (P_f) using equation (2), (3) and (4). The slope of the curves (m) was calculated by linear fitting

Table 4. Weibull parameter of tensile result

	MD90	MD45	MD30	MDQI
Shape parameter (m)	50.34	15.69	169.90	111.30
Scale parameter (σ_o), MPa	1307	254	587	723
Average strength (σ_{avg}), MPa	1292	250	584	718
% Variation between σ_o and σ_{avg}	1.15	1.38	0.36	0.72
R^2	0.97	0.96	0.98	0.98

Table 5. Weibull parameters of compressive result

	MD90	MD45	MD30	MDQI
Shape parameter (m)	59.89	27.51	32.76	111.40
Scale parameter (σ_o), MPa	616	168	217	443
Average strength (σ_{avg}), MPa	612	165	214	440
% Variation between σ_o and σ_{avg}	0.67	1.81	1.45	0.72
R^2	0.97	0.96	0.95	0.99

in the equation of straight line as given in equation (2).

$$P_f = \frac{i-0.3}{n+0.4} \tag{1}$$

$$\underbrace{\ln\left[\ln\left[\frac{1}{1-P_f}\right]\right]}_{y} = \underbrace{m\ln\sigma}_{x} - \underbrace{m\ln\sigma_o}_{\text{Intercept (c)}} \tag{2}$$

$$y = mx + c \tag{3}$$

$$\sigma_o = e^{-c/m} \tag{4}$$

The calculated Weibull parameters under tensile and compression loading are presented in Table 4 and Table 5 respectively. The shape parameter (m) was function of varying strength and reflects variation among each set of MD laminates. The four laminates were expected to illustrate varying m values due to scattered average strength caused by varying orientation. The tensile MD30 and MDQI specimens showed larger m value as compared to rest as given in Table 4. Similarly, under compression loading, MDQI showed highest m as given Table 5. This higher value of m reflected uniform statistical distribution for the aforementioned laminates [21]. The highly scatted experimental data for MD45 resulted in non-uniform distribution with the lowest m value. Various previous studies showed that a smaller value of m corresponds to the abnormal or complex final failure of the specimens [30,42]. The laminates with fibers parallel or perpendicular to loading direction generated pure tension or pure shear stress respectively. However, off-axis or cross-ply orientations confronts combined tension-shear or compression-shear stress which provides lateral support against cracks in adjacent angle plies. The combined effect of this lateral support against failure, re-orientation of

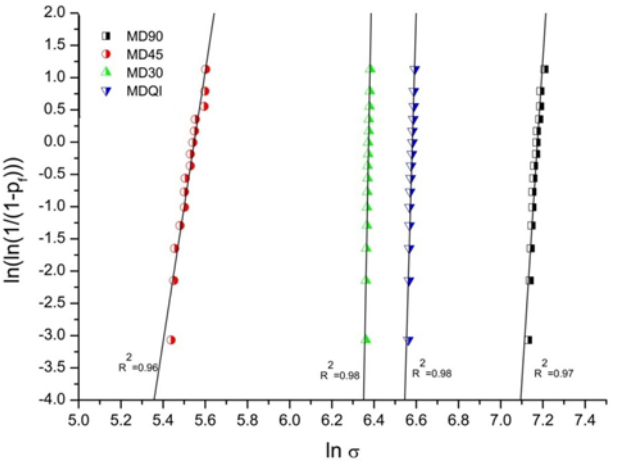

Figure 9. Weibull plot for the tensile results.

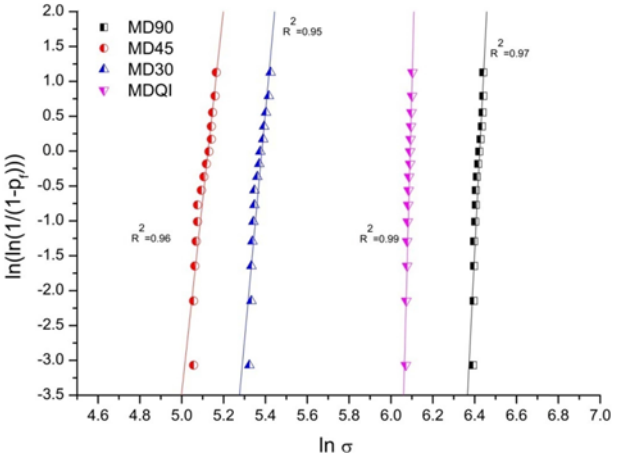

Figure 10. Weibull plot for the compressive results.

off-axis fibers, nonlinear stress-strain response and high fracture strain forced an abnormal failure in MD as compared to UD laminates [21,41]. The highest percentage variation of 1.38 % between average tensile stress (σ_{avg}) and scale parameter (σ_o) for MD45 laminate reflected higher variation between predicted and experimental results.

The MD45 and MD30 compressive specimens showed maximum variation in UCS due to the presence of angle-ply which resulted in lower m values as shown in Table 5. This also resulted in the highest percentage variation between σ_{avg} and σ_o among compression specimens due to combined split and fiber fracture. The movement of regression lines towards the right represented an increase in strength as shown in Figure 9, 10. The leftmost position of MD45 regression line under tension and compression showed its poor strengths. An excellent correlation between analytical curve fit and experimental values was achieved as approved by close to unity values of correlation coefficient (R^2).

Conclusion

An experimental investigation was carried out on macroscopic and microscopic fracture behaviour of four different carbon fiber/epoxy multidirectional laminates i.e. $(0,90,0,90)_{2S}$, $(+45,-45,+45,-45)_{2S}$, $(0,30)_{2S}$, $(+45,-45,0,90)_{2S}$ under longitudinal tensile and compressive loading. The final result was analyzed with Weibull probabilistic distribution model. Some important observations on test results are summarized below

1. The UTS and UCS decreased with increase in orientation angle for all the MD laminates.
2. The bilinear stress-strain response for MD45 and MD30 laminate was primarily due to the reorientation of off-axis fibers, lateral support against failure in adjacent plies, and high fracture strain.
3. Regardless of loading type and fiber orientation, the laminates failed parallel to the fiber direction.
4. SEM micrographs revealed domination of fiber breakage, delamination and fiber-matrix debonding in tensile specimens. Whereas matrix dominated failure like wedge shape fracture, stepped fracture, in-plane shear and kinking failure mechanism were observed in compressive micrographs.
5. The removal or crushing of tab caused by end tab stress was evident in compression specimens whereas tensile specimens were free from tabbing effect.
6. Percentage variation between average tensile stress (σ_{avg}) and scale parameter (σ_o) obtained from Weibull analysis reflected a good agreement between predicted and experimental result.

Acknowledgments

The authors express their sincere thanks to Director, VNIT, and Head of Department of Metallurgical & Materials Engineering, VNIT, Nagpur for providing testing facilities, support, and encouragement for this work. The authors gratefully acknowledge Dr. C.M. Manjunatha, Senior Principal Scientist, Structural Technologies Division, CSIR-NAL, Bangalore for his valuable guidance and advice to carry this research.

References

1. M. Kawai and T. Taniguchi, *Compos. Part A Appl. Sci. Manuf*., **37**, 243 (2006).
2. Y. Li, N. Li, J. Zhou, and Q. Cheng, *Compos. Struct*., **212**, 83 (2019).
3. M. Romanowicz, *Compos. Part B Eng*., **90**, 45 (2016).
4. M. M. Shokrieh, M. Salamat-talab, and M. Heidari-Rarani, *Theor. Appl. Fract. Mech*., **90**, 22 (2017).
5. M. Kawai and N. Itoh, *J. Compos. Mater*., **48**, 571 (2014).
6. O. I. Okoli and G. F. Smith, *J. Mater. Sci*., **33**, 5415 (1998).
7. M. Daniel and O. Ishai, "Engineering Mechanics of Composite Materials", 2nd ed., pp.316-329, Oxford University Press, New York, 2006.
8. Y. Kumagai, S. Onodera, Y. Nagumo, T. Okabe, and K. Yoshioka, *Compos. Part A Appl. Sci. Manuf*., **98**, 136 (2017).
9. D. Cai, J. Tang, G. Zhou, X. Wang, C. Li, and V. V. Silberschmidt, *Polym. Test*., **60**, 307 (2017).
10. D. Thomson, H. Cui, B. Erice, and N. Petrinic, *Compos. Part A Appl. Sci. Manuf*., **121**, 213 (2019).
11. J. Hu, C. Gao, S. He, W. Chen, Y. Li, B. Zhao, J. Chen, and D. Yang, *Compos. Struct*., **171**, 92 (2017).
12. Y. Ma, Y. Zhang, T. Sugahara, S. Jin, Y. Yang, and H. Hamada, *Compos. Part A Appl. Sci. Manuf*., **90**, 711 (2016).
13. M. S. Hussain, A. R. Anilchandra, N. Jagannathan, and C. M. Manjunatha, *Mater. Perform*., **5**, 132 (2016).
14. T. P. Philippidis and A. P. Vassilopoulos, *Int. J. Fatigue*., **21**, 253 (1999).
15. A. L. Kozlovskiy, D. I. Shlimas, I. E. Kenzhina, and M. V. Zdorovets, *Compos. Struct*., **79**, 381 (2007).
16. M. Kawai and T. Teranuma, *Compos. Part A Appl. Sci. Manuf*., **43**, 1252 (2012).
17. M. Kawai and S. Saito, *Compos. Part A Appl. Sci. Manuf*., **40**, 1632 (2009).
18. Z. Qi, Y. Liu, and W. Chen, *Compos. Struct*., **210**, 339 (2019).
19. L. Yao, H. Cui, Y. Sun, L. Guo, X. Chen, M. Zhao, and R. C. Alderliesten, *Compos. Part A Appl. Sci. Manuf*., **115**, 175 (2018).
20. P. Rosch, T. Bruder, and P. Wagner, *Mat. wiss. u. Werksttech*., **49**, 287 (2018).
21. K. W. Gan, T. Laux, S. T. Taher, J. M. Dulieu-Barton, and O. T. Thomsen, *Compos. Struct*., **184**, 662 (2018).
22. P. Maimi, P. P. Camanho, J. A. Mayugo, and A. Turon, *Mech. Mater*., **43**, 169 (2011).
23. Y. Gong, B. Zhang, S. Mukhopadhyay, and S. R. Hallett, *Compos. Struct*., **201**, 683 (2018).
24. B. X. Bie, J. Y. Huang, D. Fan, T. Sun, K. Fezzaa, X. H. Xiao, M. L. Qi, and S. N. Luo, *Carbon*, **121**, 127 (2017).
25. J. D. Fuller and M. R. Wisnom, *Compos. Part A Appl. Sci. Manuf*., **69**, 64 (2015).
26. C. Blondeau, G. Pappas, and J. Botsis, *Compos. Struct*., **216**, 464 (2019).
27. X. Deng, J. Hu, W. X. Wang, and T. Matsubara, *Compos. Struct*., **208**, 507 (2019).
28. J. Montesano, B. McCleave, and C. V. Singh, *Compos. Part B Eng*., **133**, 53 (2018).
29. W. Weibull, *J. Appl. Mech*., **18**, 293 (1951).
30. E. Barbero, J. Fernandez-Saez, and C. Navarro, *Compos. Part B Eng*., **31**, 375 (2000).
31. K. Naresh, K. Shankar, R. Velmurugan, and N. K. Gupta, *Thin Walled Struct*., **126**, 150 (2018).
32. K. Naresh, K. Shankar, and R. Velmurugan, *Compos. Part B Eng*., **133**, 129 (2018).

33. Z. Wang and Y. Xia, *Compos. Sci. Technol*., **57**, 1599 (1998).
34. ASTM D3039, "Standard Test Method for Tensile Properties of Polymer Matrix Composite Materials", ASTM International, West Conshohocken, PA, www.astm.org, 2017.
35. ASTM D3410, "Standard Test Method for Compressive Properties of Polymer Matrix Composite Materials with Unsupported Gage Section by Shear Loading", ASTM International, West Conshohocken, PA, www.astm.org, 2016.
36. P. A. Carraro and M. Quaresimin, *Int. J. Solids Struct*., **58**, 34 (2015).
37. M. J. Emerson, Y. Wang, P. J. Withers, K. Conrasdsen, A. B. Dahl, and V. A. Dahl, *Comp. Sci. Technol*., **168**, 47 (2018).
38. Z. Mahboob, I. E. Sawi, R. Zdero, Z. Fawaz, and H. Bougherara, *Compos. Part A Appl. Sci. Manuf*., **92**, 118 (2016).
39. M. Kawai, S. Yajima, A. Hachinohe, and Y. Kawase, *Compos. Sci. Technol*., **61**, 1285 (2001).
40. M. Bishara, M. Vogler, and R. Rolfes, *Compos. Struct*., **169**, 116 (2017).
41. J. Lee and C. Soutis, *Compos. Sci. Technol*., **67**, 2015 (2007).
42. M. H. Dirikolu, A. Aktas, and B. Birgoren, *Turkish J. Eng. Environ. Sci.*, **26**, 45 (2002).